Supplement of Atmos. Chem. Phys., 23, 10845–10867, 2023
https://doi.org/10.5194/acp-23-10845-2023-supplement

Atmospheric Chemistry and Physics
Open Access
EGU

Supplement of

Evaluation of aerosol- and gas-phase tracers for identification of transported biomass burning emissions in an industrially influenced location in Texas, USA

Sujan Shrestha et al.

Correspondence to: Rebecca J. Sheesley (rebecca_sheesley@baylor.edu)

1. Equivalent BC (eBC) calculation

Filter-based optical techniques of black carbon (BC) measurement do not measure the mass concentration directly but uses Mie theory to measure the light absorption coefficient of particles. The absorption coefficients (σ_{abs}) are converted into an equivalent mass concentration (eBC) using mass absorption cross section (MAC) (Eq. (1) below). Field based studies have shown a large variability in MAC values ranging from 1.6 m^2g^{-1} to 28.3 m^2g^{-1} at 550 nm (Sharma et al., 2002; Bond and Bergstrom, 2006). Large temporal and spatial variability in MAC value reported in previous studies is due to different mixing states of BC. Once emitted into the atmosphere these particles are subject to several coating processes with layers of other organic and inorganic materials (Zhao et al., 2021; Bond and Bergstrom, 2006). The coating over a core BC enhances the aerosol absorption by acting as a lens that helps in focusing more incident light on the enclosed BC core (a phenomena known as "lensing effect") (Fuller et al., 1999). This results into higher MAC value of the coated BC. Bond and Bergstrom (2006) reported MAC value of 7.5 ± 1.2 m^2g^{-1} at 550 nm for a fresh uncoated particle. But due to coating over fresh BC during local and long-range transport, the absorption can be enhanced by up to 100% (Schwarz et al., 2008; Bond and Bergstrom, 2006). Some of the commercially available instruments, however, use a fixed MAC values to obtain BC concentration, e.g., an aethalometer uses 7.77 m^2g^{-1} at 880 nm or 13.14 m^2g^{-1} at 520 nm (Drinovec et al., 2015). Use of fixed MAC values is convenient when additional collocated measurements required for MAC calculation are not available but this approach remains debatable (Zhao et al., 2021)

$$\text{eBC } (\mu g\ m^{-3}) = \frac{\sigma_{abs}\ (Mm^{-1})}{MAC\ (m^2g^{-1})} \qquad [1]$$

During the field measurement in Port Aransas, σ_{abs} was measured using Tri-color Absorption Photometer (TAP) through a $PM_{2.5}$ cyclone at three wavelengths: 365 nm, 520 nm and 640nm. Operational detail about TAP are presented elsewhere (Bernardoni et al., 2021; Ogren et al., 2017). In addition to aerosol optical measurement, a $PM_{2.5}$ bulk filter sampler was operated at Texas A&M Corpus Christi campus which is ~16 miles areal distance apart from the Port Aransas site. During the campaign, a total of six $PM_{2.5}$ bulk samples were collected. Details about the filter sample are presented in Table S1. The organic and elemental carbon (OC and EC) in the filter samples were measured using Sunset OC EC analyzer using NIOSH protocol (Schauer, 2003). Both Port Aransas and Texas A&M Corpus Christi sites have close proximity to the Gulf of Mexico and received airmasses predominantly from the East and Southeast direction during the campaign. Therefore, it is realistically more appropriate to use the MAC derived as a slope of the linear regression between σ_{abs} from TAP and EC concentration from the $PM_{2.5}$ filter samples collected during the campaign compared to using literature values. Using this method, the derived MAC at 520 nm was 11.45 ± 5.32 m^2g^{-1} which is slightly lower than that used by aethalometer (13.14 m^2g^{-1}). Mathematically, the MAC is given by the following equation:

$$\text{MAC} = \frac{\sigma_{abs}\ (Mm^{-1})}{EC\ (\mu g m^{-3})} \qquad [2]$$

where σ_{abs} is the average absorption coefficient measured by TAP at 520 nm during the $PM_{2.5}$ filter sampling period.

2. Positive Matrix Factorization of Organic Aerosol Matrix and Combined Organic and Inorganic Aerosol Matrices

To investigate the sources and processes of organic aerosols (OA), we performed positive matrix factorization (PMF) analysis on the high-resolution mass spectra (HRMS) of 1) organics only and 2) the combined spectral matrices of organic and inorganic species, respectively using the PMF2 algorithm in robust mode (Paatero and Tapper, 1994). We first generated the ion-speciated HRMS matrix and the corresponding error matrix from PIKA, and then analyzed using the PMF Evaluation Tool v3.06B (Ulbrich et al., 2009). We did PMF analysis on the entire sampling period covering both the stationary measurements and the mobile measurements.

For the organic PMF analysis, the OA data and error matrices were refined prior to PMF analysis according to the protocol summarized previously (Zhang et al., 2011; Ulbrich et al., 2009). Ions with m/z up to 190 were included in the PMF analysis. Isotopes were removed to avoid giving excess weight to their parent ions. Noisy ions were removed from the data matrix. These treatments largely improved the OA factorization but had negligible impact on the mass concentrations. A minimum error was introduced for each ion. The "bad" ions with S/N ratio < 0.2 were downweighed by increasing their error values by a factor of 10, while the "weak" ions with S/N between 0.2 and 2 were downweighed a factor of 2 as described by Ulbrich et al. (2009). O^+, OH^+, H_2O^+, and CO^+ ions were also down weighted to avoid additional weight to CO_2^+, as their signals were all scaled to that of CO_2^+. PMF solutions were tested from 2 to 7 factors, and the rotational forcing parameter, fPeak, varied between -1 and 1 (step = 0.2).

We also performed PMF analysis on the combined spectral matrices of organic and inorganic species of the HR-AMS (Zhou et al., 2017; Zhang et al., 2011; Paatero and Tapper, 1994). PMF is commonly applied to the organic mass spectral matrix to determine distinct OA factors (Zhang et al., 2011). However, conducting PMF analysis on the combined spectra of organic and inorganic aerosols allows for the derivation of additional information. In this study, we performed PMF analysis on the combined HR spectral matrices of organic and inorganic species. Organic ions at m/z 12 – 180 and major inorganic ions, i.e., SO^+, $SO2^+$, HSO_2^+, SO_3^+, HSO_3^+, and $H_2SO_4^+$ for sulfate; NO^+ and NO_2^+ for nitrate; NH^+, NH_2^+, and NH_3^+ for ammonium; and Cl^+ and HCl^+ for chloride were included, and the ion signals were expressed in nitrate-equivalent concentrations. The error matrix was pretreated the same as the PMF analysis of organic matrix only. After PMF analysis, the mass concentration of each OA factor was derived from the sum of organic signals in the corresponding mass spectrum after applying the default RIE for organics (1.4) and the time dependent CDCE. The solutions for two to nine factors were explored at a fixed rotational parameter (FPEAK = 0). We performed similar evaluation procedures as to the organic PMF analysis and chose the seven-factor solution as the optimum solution for the combined PMF analysis. Following the procedures listed in Table 1 of (Zhang et al., 2011), all PMF solutions have been evaluated by investigating the key diagnostic plots, mass spectra, correlations with external tracers and diurnal profiles. We selected the seven-factor solution with fPeak = 0 from the PMF analysis of the combined matrices as the optimum solution. The solution is presented and discussed in detail below.

After a detailed evaluation of temporal trends, mass spectral profiles, and correlations with ions, we identified seven distinct OA factors. These seven factors are: 1) hydrocarbon-like organic aerosol (HOA) that is associated with traffic related primary emission, 2) biomass burning organic aerosol (BBOA) associated with campfires as well as regional transported wildfire plumes, 3) less-oxidized oxygenated organic aerosol (LO-OOA) representing less processed and

fresher secondary organic aerosol (SOA) (O/C = 0.51), 4) more-oxidized OOA (MO-OOA) possibly representing more processed and aged SOA (O/C = 1.22), 5) an OOA that was associated with ammonium nitrate and biomass burning (AN-BB-OOA), 6) a highly oxidized OOA associated with ammonium sulfate (AS-OOA), and 7) a highly oxidized OOA associated with acidic sulfate (acidic-OOA). Three of these factors had inorganic signals in the mass spectra, and were associated with neutralized ammonium nitrate, neutralized ammonium sulfate, and acidic sulfate signals, respectively.

Table S1. Details about $PM_{2.5}$ filter samples collected at Texas A&M Corpus Christi

Sample ID	Start Date	Start Time	End Date	End Time
210403_MV2.5_COR	4/3/21	10:06	4/6/21	17:02
210406_MV2.5_COR	4/6/21	19:19	4/9/21	18:43
210409_MV2.5_COR	4/9/21	18:59	4/13/21	11:41
210413_MV2.5_COR	4/13/21	11:48	4/16/21	18:21
210416_MV2.5_COR	4/16/21	18:38	4/20/21	17:01
210420_MV2.5_COR	4/20/21	17:07	4/22/21	11:34

Table S2. The 1-min and 2.5-min minimum detection limits (MDL) of the measured nonrefractory submicron aerosol species during the sampling campaign, which were determined as three times the standard deviation (3σ) of the corresponding signals in particle-free ambient air.

Species	MDL- 2.5 min (μg m^{-3})
Organics	0.37
Sulfate	0.072
Nitrate	0.02
Ammonium	0.063
Chloride	0.024

Table S3. Minimum detection limit (MDL) for 30-s averaged data and associated uncertainty for trace gas measurements.

Species	Uncertainty (%)	MDL (ppbv)
CO	1.4	0.13
CO_2	1	0.33
NO	4.7	0.07
NO	4.5	0.35
NO_2	5.4	0.13
NO_2	9.3	0.49
NO_y	5.6	0.48
O_3	1.9	0.23
SO_2	9.1	0.92

Table S4. Minimum detection limit (MDL) in ppbv and uncertainty associated with the measured VOCs during the sampling campaign.

Species	**m/z**	**Uncertainty (%)**	**MDL (ppbv)**
Formaldehyde	31	10.8	0.66
Acetonitrile	42	10.7	0.09
Acetaldehyde	45	9.6	0.26
Acetone	59	20.9	0.42
DMS	63	9.6	0.15
Isoprene	69	10.1	0.15
MVK+MACR	71	9.5	0.16
MEK	73	9.6	0.12
Benzene	79	9.9	0.13
Toluene	93	9.9	0.16
Monoterpene	137	11.2	0.52
Hydroxyacetone	75	16.7	0.44
Styrene	105	11.4	0.1
Xylene	107	11.1	0.18

Figures

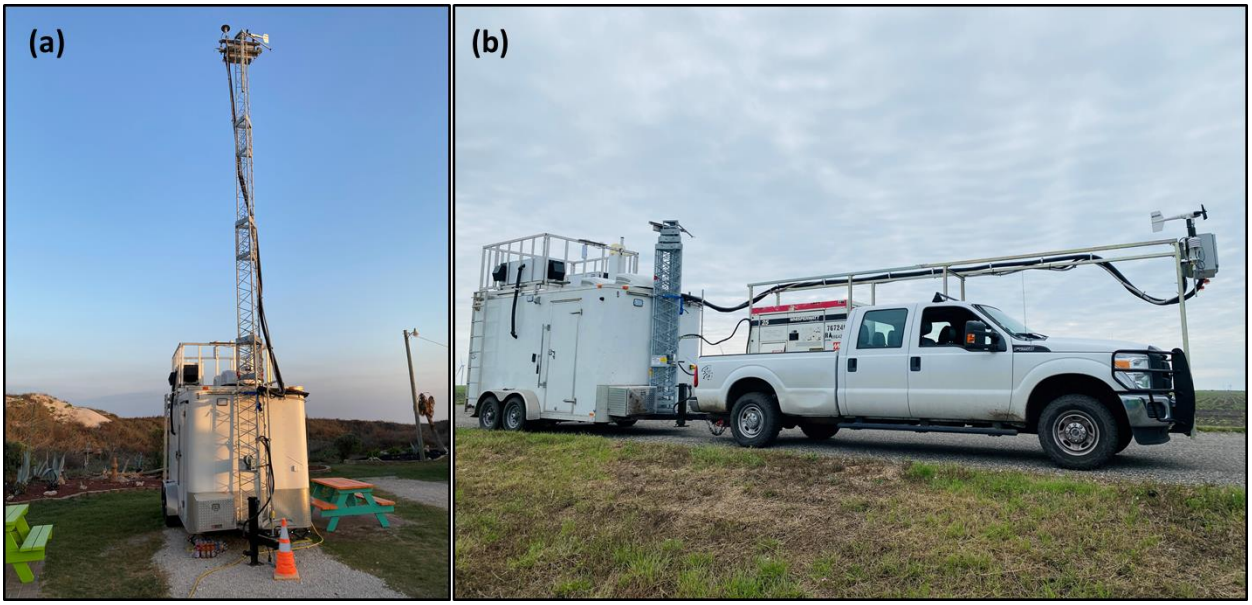

Fig. S1. Mobile air quality laboratory (MAQL2) during **(a)** stationary phase and **(b)** mobile phase.

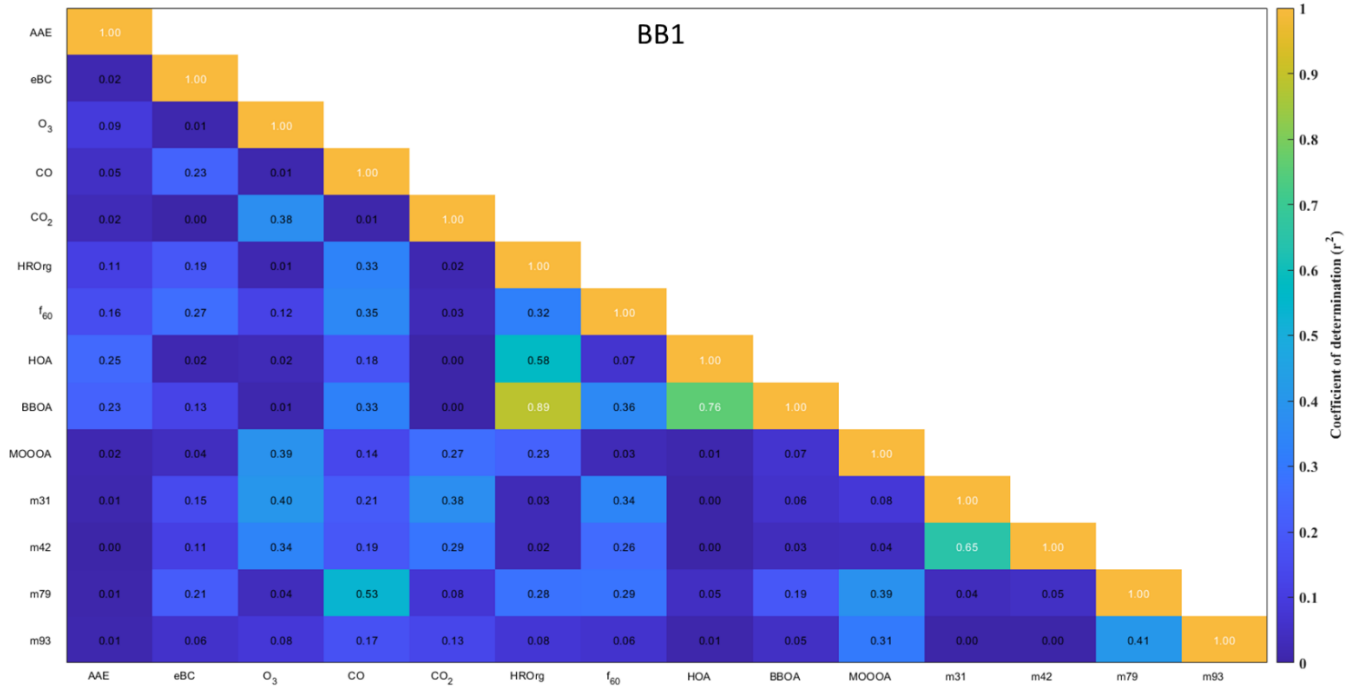

Fig. S2. Correlation plot of select-aerosol optical properties, trace gases, aerosol composition and VOCs during BB1.

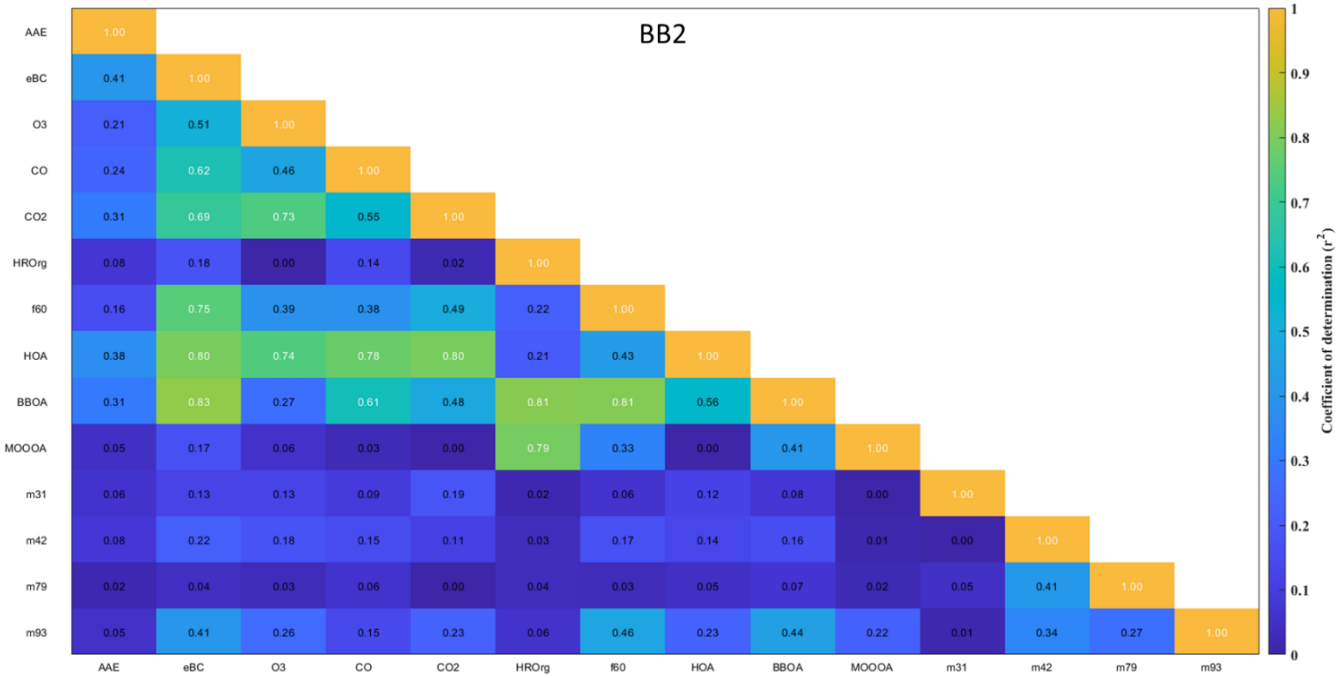

Fig. S3. Correlation plot of select-aerosol optical properties, trace gases, aerosol composition and VOCs during BB2.

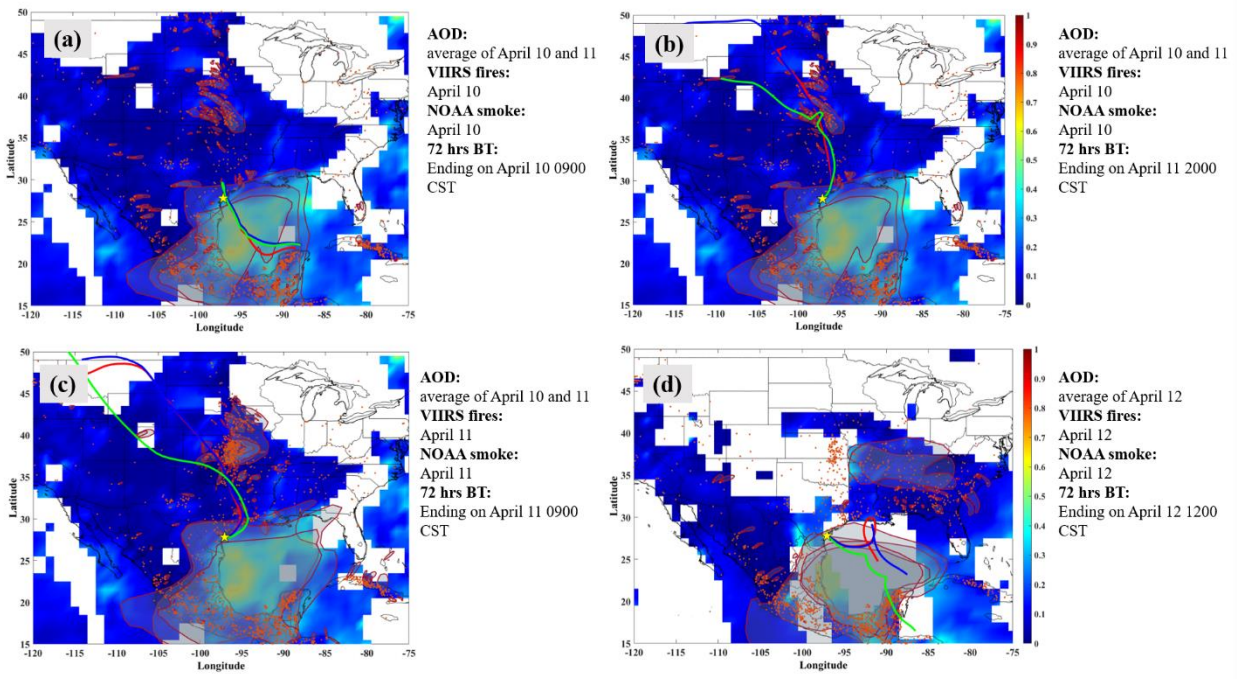

Fig. S4. Spatial distribution of average Aerosol Optical Depth (AOD) from Aqua and Terra satellites (April 10 – 12, 2021). Visible Infrared Imaging Radiometer Suite (VIIRS) active fire, NOAA Hazard Mapping System (HMS) smoke and HYSPLIT Backward trajectories (BTs) at different starting heights: 50 m (red), 100 m (blue) and 500 m (green) are included in the map. The ending times of the BTs are chosen to show the gradual change in the path of BTs from the Central Mexico to the Northern US during the period of interest in this study. The study site Port Aransas is denoted by a yellow star symbol.

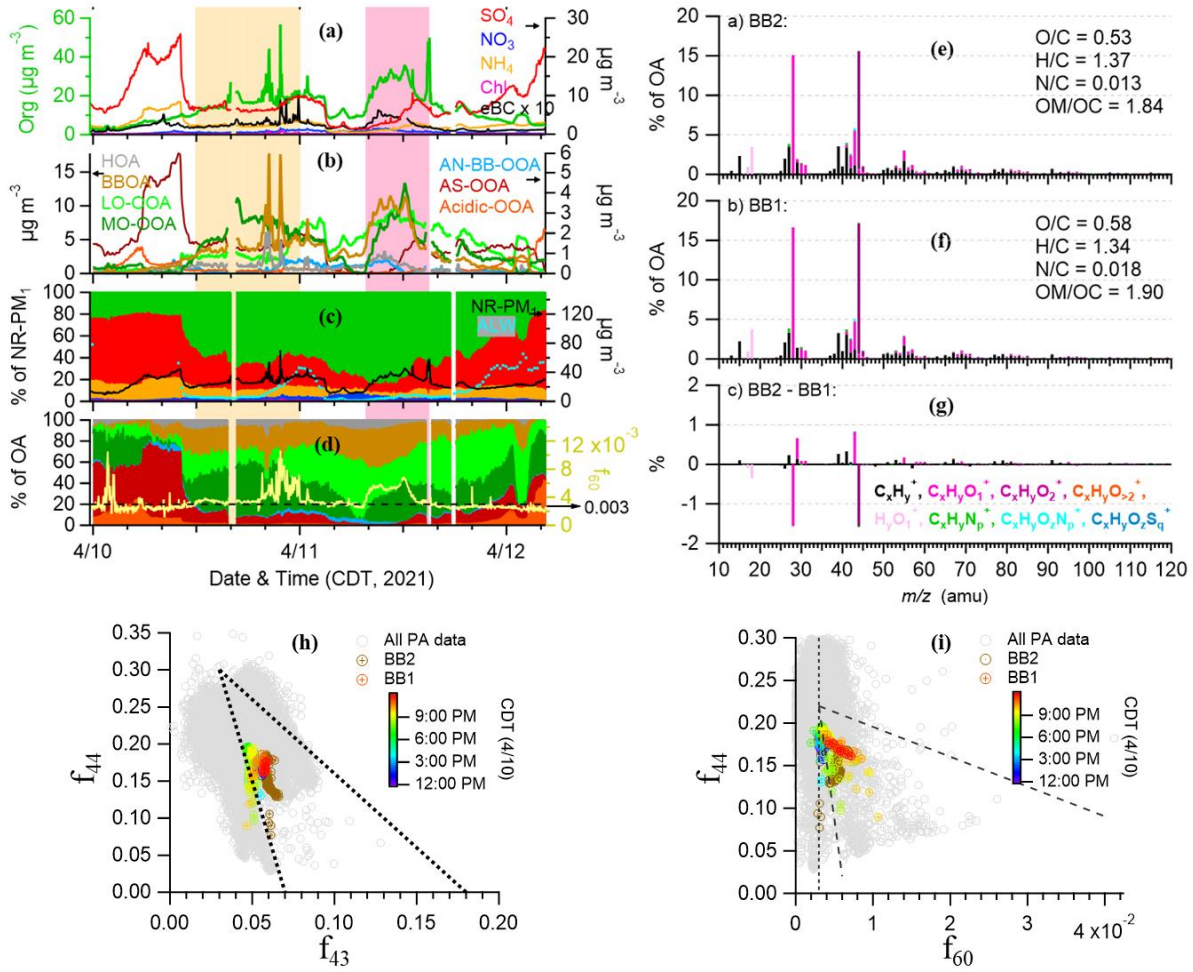

Fig. S5. Time series of **(a)** mass concentrations of NR-PM_1 species, **(b)** mass concentrations of OA factors determined from PMF analysis, **(c)** NR-PM_1 composition, **(d)** OA composition and f_{60} (i.e., $C_2H_4O_2^+$ / OA) is the yellow lines, and; **(e-g)** high resolution mass spectra (HRMS) of OA during two BB periods and the difference HRMS colored by eight ion families at m/z < 120. The seven PMF factors in panel **(b)** include: i) hydrocarbon-like organic aerosol (HOA), ii) BB OA (BBOA), iii) less-oxidized oxygenated OA (LO-OOA), iv) more-oxidized OOA (MO-OOA), v) less oxidized OOA associated with ammonium nitrate and biomass burning (AN-BB-OOA), vi) highly oxidized OOA associated with ammonium sulfate (AS-OOA), and vii) highly oxidized OOA associated with acidic sulfate (acidic-OOA). The dashed black line in panel **(d)** indicates f_{60} = 0.3%. The elemental ratios of OA determined by the Aiken-Ambient method (Aiken et al., 2008) are shown in the legends of panels (**e-f**). Scatterplot of f_{44} vs. f_{60} **(i)** and f_{44} vs. f_{60} **(j)** where BB1 data are colored as a function of time of the day. The grey markers correspond to the measured OA during this study. The triangular boundaries set in panel **i** and panel **j** represent the ranges observed in ambient OOA field data from literature (Cubison et al., 2011; Ng et al., 2010)

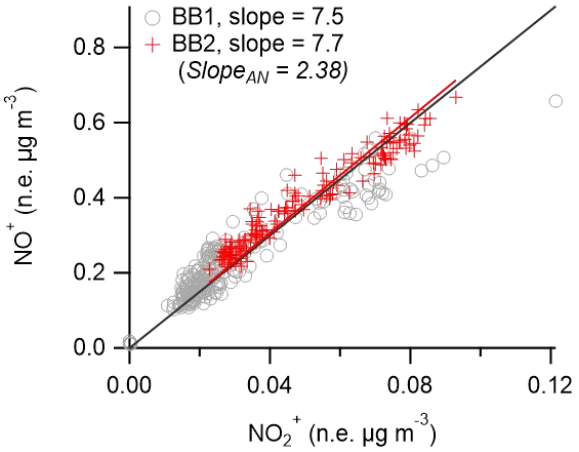

Fig. S6. Scatter plot between NO^+ and NO_2^+ measured by the HR-ToF-AMS during BB1 and BB2. Data fitting was performed using orthogonal distance regression.

References

Aiken, A. C., DeCarlo, P. F., Kroll, J. H., Worsnop, D. R., Huffman, J. A., Docherty, K. S., Ulbrich, I. M., Mohr, C., Kimmel, J. R., Sueper, D., Sun, Y., Zhang, Q., Trimborn, A., Northway, M., Ziemann, P. J., Canagaratna, M. R., Onasch, T. B., Alfarra, M. R., Prevot, A. S. H., Dommen, J., Duplissy, J., Metzger, A., Baltensperger, U., and Jimenez, J. L.: O/C and OM/OC Ratios of Primary, Secondary, and Ambient Organic Aerosols with High-Resolution Time-of-Flight Aerosol Mass Spectrometry, Environ. Sci. Technol., 42, 4478–4485, https://doi.org/10.1021/es703009q, 2008.

Bernardoni, V., Ferrero, L., Bolzacchini, E., Forello, A. C., Gregorič, A., Massabò, D., Močnik, G., Prati, P., Rigler, M., Santagostini, L., Soldan, F., Valentini, S., Valli, G., and Vecchi, R.: Determination of Aethalometer multiple-scattering enhancement parameters and impact on source apportionment during the winter 2017/18 EMEP/ACTRIS/COLOSSAL campaign in Milan, Atmos. Meas. Tech., 14, 2919–2940, https://doi.org/10.5194/amt-14-2919-2021, 2021.

Bond, T. C. and Bergstrom, R. W.: Light absorption by carbonaceous particles: An investigative review, Aerosol Sci. Technol., 40, 27–67, https://doi.org/10.1080/02786820500421521, 2006.

Cubison, M. J., Ortega, A. M., Hayes, P. L., Farmer, D. K., Day, D., Lechner, M. J., Brune, W. H., Apel, E., Diskin, G. S., Fisher, J. A., Fuelberg, H. E., Hecobian, A., Knapp, D. J., Mikoviny, T., Riemer, D., Sachse, G. W., Sessions, W., Weber, R. J., Weinheimer, A. J., Wisthaler, A., and Jimenez, J. L.: Effects of aging on organic aerosol from open biomass burning smoke in aircraft and laboratory studies, Atmos. Chem. Phys., 11, 12049–12064, https://doi.org/10.5194/acp-11-12049-2011, 2011.

Drinovec, L., Močnik, G., Zotter, P., Prévôt, A. S. H., Ruckstuhl, C., Coz, E., Rupakheti, M., Sciare, J., Müller, T., Wiedensohler, A., and Hansen, A. D. A.: The "dual-spot" Aethalometer: An improved measurement of aerosol black carbon with real-time loading compensation, 1965–1979 pp., https://doi.org/10.5194/amt-8-1965-2015, 2015.

Fuller, K. A., Malm, W. C., and Kreidenweis, S. M.: Effects of mixing on extinction by carbonaceous particles, J. Geophys. Res. Atmos., 104, 15941–15954, https://doi.org/10.1029/1998JD100069, 1999.

Ng, N. L., Canagaratna, M. R., Zhang, Q., Jimenez, J. L., Tian, J., Ulbrich, I. M., Kroll, J. H., Docherty, K. S., Chhabra, P. S., Bahreini, R., Murphy, S. M., Seinfeld, J. H., Hildebrandt, L., Donahue, N. M., DeCarlo, P. F., Lanz, V. A., Prévôt, A. S. H., Dinar, E., Rudich, Y., and Worsnop, D. R.: Organic aerosol components observed in Northern Hemispheric datasets from Aerosol Mass Spectrometry, Atmos. Chem. Phys., 10, 4625–4641, https://doi.org/10.5194/acp-10-4625-2010, 2010.

Ogren, J. A., Wendell, J., Andrews, E., and Sheridan, P. J.: Continuous light absorption photometer for long-term

studies, Atmos. Meas. Tech., 10, 4805–4818, https://doi.org/10.5194/amt-10-4805-2017, 2017.

Paatero, P. and Tapper, U.: Positive matrix factorization: A non-negative factor model with optimal utilization of error estimates of data values, Environmetrics, 5, 111–126, https://doi.org/10.1002/env.3170050203, 1994.

Schauer, J. J.: Evaluation of elemental carbon as a marker for diesel particulate matter, J. Expo. Sci. Environ. Epidemiol., 13, 443–453, https://doi.org/10.1038/sj.jea.7500298, 2003.

Schwarz, J. P., Spackman, J. R., Fahey, D. W., Gao, R. S., Lohmann, U., Stier, P., Watts, L. A., Thomson, D. S., Lack, D. A., Pfister, L., Mahoney, M. J., Baumgardner, D., Wilson, J. C., and Reeves, J. M.: Coatings and their enhancement of black carbon light absorption in the tropical atmosphere, J. Geophys. Res., 113, D03203, https://doi.org/10.1029/2007JD009042, 2008.

Sharma, S., Brook, J. R., Cachier, H., Chow, J., Gaudenzi, A., and Lu, G.: Light absorption and thermal measurements of black carbon in different regions of Canada, J. Geophys. Res. Atmos., 107, https://doi.org/10.1029/2002JD002496, 2002.

Ulbrich, I. M., Canagaratna, M. R., Zhang, Q., Worsnop, D. R., and Jimenez, J. L.: Interpretation of organic components from Positive Matrix Factorization of aerosol mass spectrometric data, Atmos. Chem. Phys., 9, 2891–2918, https://doi.org/10.5194/acp-9-2891-2009, 2009.

Zhang, Q., Jimenez, J. L., Canagaratna, M. R., Ulbrich, I. M., Ng, N. L., Worsnop, D. R., and Sun, Y.: Understanding atmospheric organic aerosols via factor analysis of aerosol mass spectrometry: a review, Anal. Bioanal. Chem., 401, 3045–3067, https://doi.org/10.1007/s00216-011-5355-y, 2011.

Zhao, W., Tan, W., Zhao, G., Shen, C., Yu, Y., and Zhao, C.: Determination of equivalent black carbon mass concentration from aerosol light absorption using variable mass absorption cross section, Atmos. Meas. Tech., 14, 1319–1331, https://doi.org/10.5194/amt-14-1319-2021, 2021.

Zhou, S., Collier, S., Jaffe, D. A., Briggs, N. L., Hee, J., Sedlacek III, A. J., Kleinman, L., Onasch, T. B., and Zhang, Q.: Regional influence of wildfires on aerosol chemistry in the western US and insights into atmospheric aging of biomass burning organic aerosol, Atmos. Chem. Phys., 17, 2477–2493, https://doi.org/10.5194/acp-17-2477-2017, 2017.